Journal of Power Sources 241 (2013) 203–211

Contents lists available at SciVerse ScienceDirect

Journal of Power Sources

journal homepage: www.elsevier.com/locate/jpowsour

Expanded polytetrafluoroethylene reinforced polyvinylidenefluoride–hexafluoropropylene separator with high thermal stability for lithium-ion batteries

Ming Xiong, Haolin Tang*, Yadong Wang, Yu Lin, Meiling Sun, Zhuangfei Yin, Mu Pan

State Key Laboratory of Advanced Technology for Materials Synthesis and Processing, Wuhan University of Technology, Wuhan 430070, PR China

HIGHLIGHTS

- Porous polytetrafluoroethylene stabled separator for Li-ion battery.
- Highly thermal stability and low thermal shrinkage.
- Excellent capacities at high rate discharge.

ARTICLE INFO

Article history:
Received 5 December 2012
Received in revised form
10 April 2013
Accepted 15 April 2013
Available online 30 April 2013

Keywords:
Separator
Polyvinylidenefluoride
–hexafluoropropylene
Expanded polytetrafluoroethylene
Thermal shutdown
Thermal shrinkage

ABSTRACT

PVDF–HFP/ePTFE composite separator with high thermal stability and low thermal shrinkage characteristic has been developed. The PVDF–HFP acts to absorb the electrolyte and shutdown at elevated temperature. The thermally stable ePTFE matrix is adopted to improve the mechanical strength and sustain the insulation after the shutdown. This novel separator presents good ion conductivity (up to 1.29 mS cm^{-1}) and has a low thermal shrinkage of 8.8% at 162 °C. The composite separator shutdown at 162 °C and keep its integrity before 329 °C. Cells based on the composite separator show excellent capacities at high rate discharge and stable cycling performance.

1. Introduction

The application of lithium-ion batteries has been expanding from electronic devices to power tools and electric vehicles, due to their high capacity and long cycle life. Intensive research has been conducted to improve the performance of lithium batteries, such as energy densities and abuse tolerance of batteries. Among them, safety presents a critical challenge and numerous methods have been developed to suppress the failure [1–3].

The separator in a battery plays an important role to retain electrolyte, prevent shortage between the two electrodes while maintaining high ion permeation, and to perform safe deactivation of the cell under overcharge, abnormal heating or mechanical rupture conditions [4]. Currently widely used separators in lithium-ion batteries are most commonly fabricated by polyolefins such as polypropylene (PP) and polyethylene (PE), which will shrink or melt at elevated temperatures and cause an internal short-circuit, as well as poor in wettability. In order to overcome these limitations, various approaches have been addressed, Such as impregnation of gel polymer electrolytes into nonwovens [5–8], coating of gel polymer or ceramic powders to polyolefin separators [9–15], and other fabrication techniques [16–20]. Although improvement in thermal shrinkage and wettability has been observed, further improvement is still desired for applications which require more safety assurance. For example, when the internal temperature of the power battery excessively increases, the porous separator should partially melt to clog its micropores, which increases the impedance of the battery and consequently prevents the further reaction. Moreover, this shutdown state should be continuously maintained before the cooling down of the battery, and a wide shutdown window is necessary.

* Corresponding author. Tel.: +86 27 8788 4448; fax: +86 27 8787 9468.
E-mail address: thln@whut.edu.cn (H. Tang).

0378-7753/$ – see front matter © 2013 Elsevier B.V. All rights reserved.
http://dx.doi.org/10.1016/j.jpowsour.2013.04.064

In this study, a composite separator comprising a microporous polyvinylidenefluoride–hexafluoropropylene (PVDF–HFP) layer and an expanded polytetrafluoroethylene (ePTFE) matrix support was developed. The PVDF–HFP serves to absorb the liquid electrolyte and shutdown at elevated temperature. The ePTFE matrix acts to reinforce the mechanical strength and keep the integrity to prevent short-circuit after the shutdown of PVDF–HFP layer. The porosity of composite separator is determined by controlling the content of pore-forming agent (PEG). Mechanical, thermal and electrochemical properties, as well as the morphology of the composite separators have been studied systematically. The contents of PEG have also been changed to understand the effects of these variables on the properties of prepared separators.

2. Experimental

2.1. Preparation of composite separators

PVDF–HFP with an average molecular weight of 450,000 (pellets, Aldrich, USA), polyethylene glycol (PEG) with an average molecular weight of 20,000 (Sinopharm Chemical Reagent Co., Ltd.), other solvents were reagent grade and used as received.

To prepare the casting solution, 8 g of PVDF–HFP was dissolved in a 60 ml mixture of high boiling-point solvent (DMF) and volatile solvent (acetone) with the volume ratio of 1–2. Due to the low surface energy of ePTFE matrix, the proportion of the high boiling-point solvent is low enough to allow the wetting of ePTFE and high enough to allow phase separation during evaporation [21]. In the PVDF–HFP solution, various amounts of PEG were added under vigorous stirring at 60 °C for 12 h (the weight ratios of PEG/PVDF–HFP were 30%, 50%, 70%, 90% and 110%, respectively).

Porous ePTFE membranes (porosity = 85%, thickness = 6 μm, pore size = 1–2 μm, Dagong Co., Shanghai, China) were used as the matrix of the composite separator. The matrix membrane was first mounted on 10 cm × 10 cm plastic frame and dried in a vacuum oven at 60 °C for 1 h to remove water. The frame was laid in a Petri dish. The casting solution was poured on the ePTFE matrix. The Petri dish was sealed at 30 °C for 30 min for impregnation. Then the impregnated membrane was dried at 100 °C in a vacuum oven for 6 h to remove the organic solvents. The composite separator was immersed in a pool of deionized water for 12 h to remove the PEG from PVDF–HFP and generate porous structure. The separator was then dried at ambient temperature.

2.2. Characterization of the composite separators

2.2.1. Morphology of composite separators

The morphologies of separators were examined using a field emission scanning electron microscope (FE-SEM, S-4800, Hitachi). The tensile strength was determined by using a Tensile Tester (Hualong WDW-0.5). The electrolyte uptake and porosity are measured by immersing the membrane into n-butanol and liquid electrolyte separately for 30 min and calculating with the following equation:

$$\text{Posority}(\%) = 100 \times \frac{M_x/\rho_x}{M_x/\rho_x + M_y/\rho_y}$$

$$\text{Electrolyte uptake}(\%) = 100 \times \frac{W_i - W_o}{W_o}$$

where M_x and M_y are the weight of n-butanol absorbed and the dried composite separator, respectively. ρ_x and ρ_y are the density of n-butanol and the dried composite separator, respectively. The density of composite separator was determined by measuring the volume and the weight. W_i was the weight of the wet separator soaked with electrolyte and W_o was the weight of dry separator. The extra solution (n-butanol or electrolyte) at the surface of the separator was absorbed with a filter paper before measuring weight.

2.2.2. Thermo shrinkage and shutdown property

DSC and TGA scans were performed with a simultaneous TG-DSC system (STA 449F3, NETZSCH) at the rate of 5 °C min^{-1} under nitrogen purge from 30 °C to 350 °C. TMA tests were performed on a TMA analyzer (TMA202, NETZSCH) under N_2 atmosphere and the temperature was increased 5 °C min^{-1} from 30 °C to 200 °C, with a constant external tensile force of 0.02 N. A heat plate is used to present the thermo shrinkage instantaneously.

To prepare the cell for high temperature test, the cell was assembled by sandwiching the separator between a MCMB (Mesophase Carbon Micro Beads) anode and a $LiFePO_4$ cathode and then activated by filling liquid electrolyte. Then it was sealed in a CR2032 shell with the pressure of 50 kg cm^{-2} by using a sealing machine (MSK-110, MTI Corp.). All the cells were first charged to 75% state of charge (SOC) using battery test equipment (CT2001A, LAND Electronics) and were left at OCV condition for 24 h, and then was heated in a heating mantle from room temperature to around 200 °C at which the OCV drops to zero. The temperature is increased at the rate of 10 °C min^{-1} and was measured with a thermometer (YC-727UD, Tenmars) by attaching the thermocouple to the cell surface. The OCV was measured using an electrochemical workstation (CHI604D, CH Instruments).

2.2.3. Electrochemical measurements

The composite separators were sufficiently soaked in a liquid electrolyte in an Ar-filled glove box. The electrolyte contained 1 M LiPF6 in ethylene carbonate (EC)–diethyl carbonate (DEC)–ethyl methyl carbonate (EMC) ($v/v/v$ = 1/1/1, Samsung Cheil Industries). The soaked separators were sandwiched between two stainless steel electrodes and assembled into a tightly sealed test cell. The ionic conductivity at various temperatures was determined by an AC impedance analysis using an electrochemical workstation (CHI604D, CH Instruments) over the frequency range of 10 Hz–10^5 Hz and under an AC voltage of 5 mV. It was calculated from the following equation:

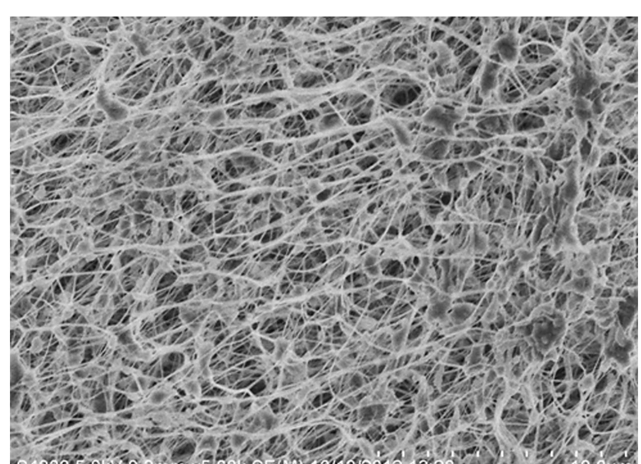

Fig. 1. FE-SEM photographs (surface) of pristine ePTFE matrix.

$$\sigma = \frac{d}{R \cdot S}$$

where σ is the ionic conductivity, d is the thickness of the composite separator, R is the bulk resistance, and S is the area of the electrode.

The composite separators for the electrochemical stability measurement were sandwiched between lithium metal and stainless steel electrodes in a test cell. And then the electrochemical stability was measured by using a liner sweep voltammetry from 2.5 V to 5.5 V at 2 mV s^{-1}.

The charge/discharge and cyclability tests of cells were performed using battery test equipment (CT2001A, LAND Electronics). A half-cell was assembled by sandwiching the separator between a lithium anode and a $LiFePO_4$ cathode and then activated by filling liquid electrolyte. The discharge current densities were varied from 0.1 C to 2 C under a voltage range between 2.5 V

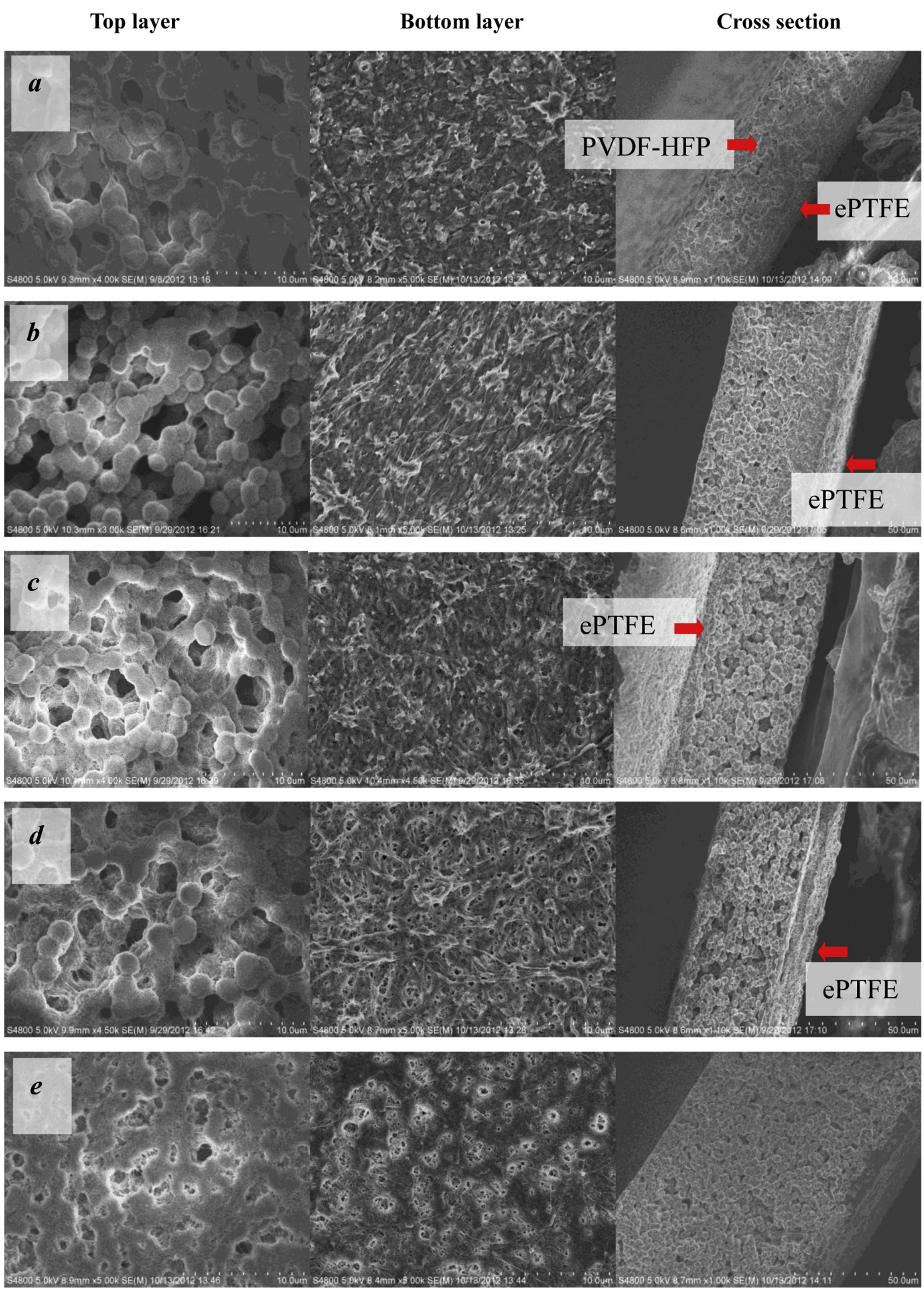

Fig. 2. FE-SEM photographs for PVDF–HFP/ePTFE composite separators as a function of PEG removal: (a) 30%; (b) 50%; (c) 70%; (d) 90%; (e) 110%.

and 4 V. The cells were cycled at a fixed charge/discharge current density of 0.1 C.

3. Results and discussion

3.1. Membrane characteristics of the composite separator

The pristine ePTFE matrix shows a mesh structure containing large sized pores (Fig. 1). Fig. 2(a)–(e) shows that the composite separator has an asymmetric structure with two layers. The bottom layer of about 6 μm thick is composed by ePTFE permeated with PVDF–HFP. The top layer is a porous PVDF–HFP coating of about 50 μm thick. Cross-sectional morphology of the composite separator indicates that the PVDF–HFP particles are compactly merged with ePTFE matrix. The interlinked crystalline particles morphology of top layer indicates that solid–liquid demixing occurred in the crystallizable segments of the polymer [22,23].

Fig. 2(a)–(e) demonstrates that the number of pores in the surface and cross-section of composite separator increases with the increasing PEG content up to 90%. It has also been confirmed by the result of measurement of porosity showed in Fig. 3. A similar observation has been reported by Hwang et al. [24]. However, as the content of PEG increases from 90% to 110%, dense skin layers on both sides of membrane are formed, which block some pores on the surface and consequently decreased the porosity. Based on the mechanism of the skin layer, it is probable that the proportion of solvent decreases as the content of polymers increasing. Thus the quickly vaporization of solvent at the surface leads to the formation of the amorphous skin layer [25].

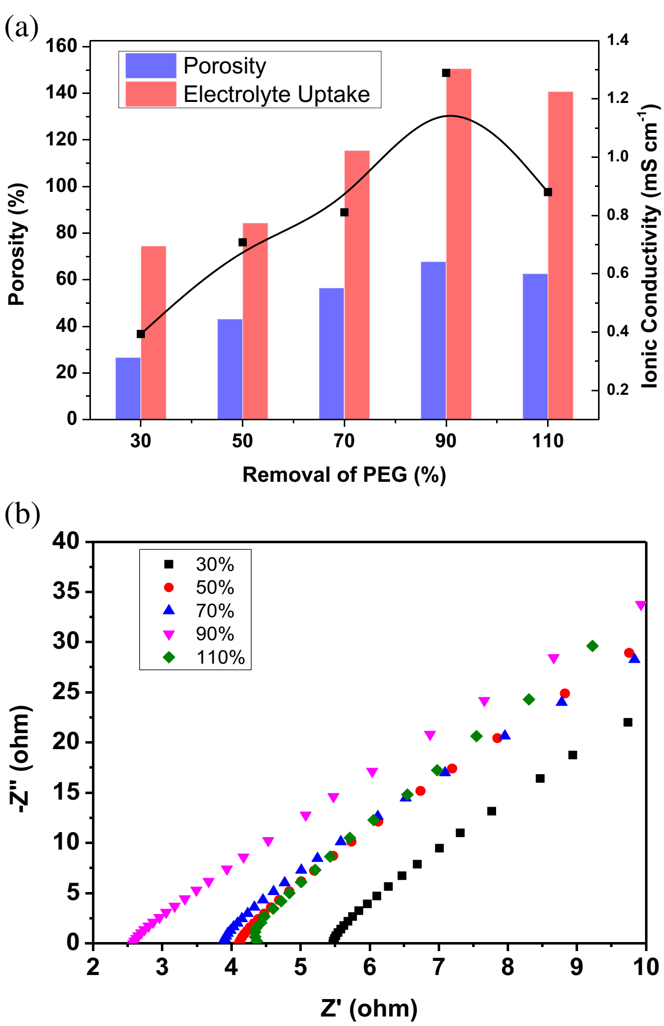

Fig. 3. (a) Ionic conductivity, porosity and electrolyte uptake of composite separator as a function of removal of different of wt.% of PEG. (b) The AC impedance spectra of symmetric cells SS/separator/SS with the composite separator.

Fig. 3(a) illustrates that the ion conductivity as well as porosity and electrolyte uptake of composite separator increase with the PEG content until it reaches a maximum when 90 wt.% of PEG is removed. According to the previous research, the ionic conductivity of a porous membrane depends on the conductivity of the electrolyte embedded in the pores of the membrane [26]. Hence, when the removal of PEG is increased, the porosity of the composite separator increases from 27% to 68%, which in turn increases the amount of uptake of liquid electrolyte from 75% to 151%. Consequently, it increases the ionic conductivity. However, the porosity begins to decrease while more PEG is removed. The porosity of composite separator with 110% PEG removal is lower than the one with 90% PEG removal due to the skin layers generated as is shown in Fig. 2(e), leading to a decrease in electrolyte uptake and ion conductivity. The AC impedance spectra and the parameters of the cells with the composite separators are shown in Fig. 3(b) and Table 1, respectively. As can be seen from the spectra, the cell with 90% PEG removal composite separator has the lowest resistance of 2.6 Ω leading to the highest ionic conductivity. In this study, the composite separator with 90% PEG removal is used for electrochemical test as it has the highest ion conductivity of 1.29 mS cm^{-1}.

Fig. 4 presents the temperature dependent ionic conductivity of composite separator. It can be observed that the ionic conduction versus temperature in the composite separators obey the Arrhenius equation. It should be noticed that when the temperature reaches 120 °C, the conductivity of the composite separator with 110% PEG removal plummets. It can be ascribed to the fact that at this temperature the amorphous skin layers on the surface melt prior to crystalline particles and the membrane loses its consistency [27]. Meanwhile, the interlinking particulate morphology of other separators with different content of PEG removal remains stable which makes their conductivity consistently increases up to 120 °C. This is attributed to the fact that the fluidity of the polymers is limited by crystalline particles which makes them suitable for high temperature use [27].

Fig. 5 shows the stress–strain curves of composite separators as well as for the bare PVDF–HFP membrane. Commonly, the tensile strength of bare PVDF–HFP membrane with high porosity could not meet the requirement of winding machines (1000 psi or 6.9 MPa) [28]. In addition, PVDF–HFP loses its mechanical strength in a liquid electrolyte, especially when the temperature is high, which may result in an increased risk of electric short when highly porous PVDF membranes are used as separators [29]. However, with the existing of ePTFE, the tensile strength of composite separator has been greatly increased. As seen in Fig. 5, the fracture strength and elongations of all composite separators are significantly higher than that of the bare PVDF–HFP membrane (without

Table 1
Cell parameters for the measuring of ionic conductivity.

Percentage of PEG removal	Resistance, Ω	Thickness, μm	Area, cm^2	Ionic conductivity at 30 °C, mS cm^{-1}
30%	5.5	40	1.85	0.393
50%	4.2	55	1.85	0.708
70%	4	60	1.85	0.811
90%	2.6	62	1.85	1.289
110%	4.3	70	1.85	0.880

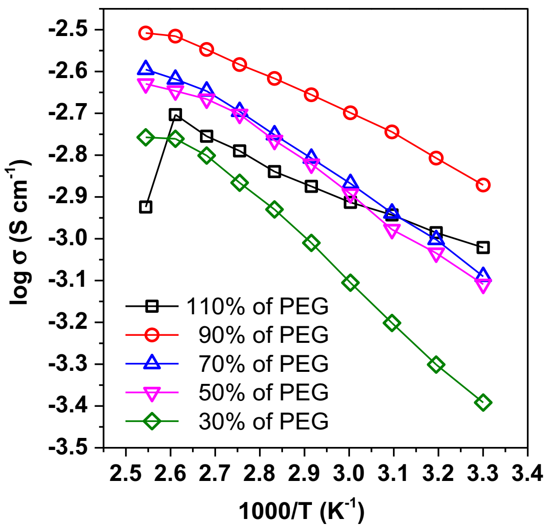

Fig. 4. Temperature dependence of ionic conductivity of composite separator.

ePTFE matrix), which is broken at only 5.38 MPa tensile stress and 4.42% elongation. The mechanical properties of composite separators depend on the content of PEG removal. With the increase of PEG removal content from 30% to 110%, the fracture strength decreases from 20.45 MPa to 9.63 MPa. The decrease in tensile strength is attributed to the higher porosity which weakens the linkage between the polymer particles.

3.2. Shutdown property

Lithium secondary batteries will initiate self-heating in abnormal situations, such as overcharging and internal/external short-circuit [30]. Therefore, thermal shutdown by separators is a useful mechanism for avoiding thermal runaway reactions in Li-ion batteries. In principle most polyolefinic separators are shutdown separators since they melt at reasonable (<200 °C) temperatures, such as polypropylene separators which shutdown at around 170 °C, and polyethylene separators which shutdown between 130 °C and 140 °C [31].

Fig. 6 shows the TGA and DSC curves of PVDF–HFP pellets and composite separators. The melting peaks of the PVDF–HFP pellets as well as composite separators are both at around 161 °C, which suggest that the crystal form of the PVDF–HFP is maintained during the membrane formation. No other phase changes are found for composite separators before temperature increases up to 329 °C. TGA curve also shows that the PVDF–HFP and composite separators are thermally stable at the temperature lower than 340 °C.

The impedance of composite separators was measured from 30 °C to 162 °C, as shown in Fig. 7. For composite separators, the sharp impedance rise appeared at around 162 °C and increased by two or three orders of magnitude. The composite separators would maintain thermal stability up to 329 °C as have been revealed by DSC curve, to prevent the safety hazard caused by the continuing rise of temperature before actually cooling down. The AC impedance spectra show the same trend when the temperature increased to the melting point of PVDF–HFP. In Fig. 7(b), some scattered data points appeared in high frequency range, it might be caused by the instable state of the composite separator which was on the process of melting. At the melting point, violent morphological change is happening and making some disturbance on the impedance test to some extent.

In order to study the performance of cell with composite separators, the open-circuit voltage (OCV) of the cell as a function of temperature was also investigated (Fig. 7). The OCV maintained nearly the same as the temperature increased to 175 °C, which means the melting of PVDF–HFP did not cause an internal short-circuit. However, a fluctuation in OCV appeared between 180 °C and 190 °C, followed by a quick drop to zero at around 200 °C. The observed fluctuation and drop in OCV are hard to explain and may be due to the temperature induced changes in active electrode materials and electrolyte, or the formation of pinholes in the separator [32]. At the end of this test, all the cells are ruptured and broke apart at the joint of the positive and negative shell. These results could be attributed to the volumetric expansion of electrolyte gases at high temperature, which in turn caused the irreversible deformation of the metal shell [33]. A recovery of the OCV at the end of the test also indicates the cell venting when the vapor pressure of electrolyte broke the shell [32].

Fig. 8 shows the morphologies after the shutdown of composite separators. It can be seen from the surfaces and cross-sections that the interlinking spherical particles melted and collapsed to clog the micropores, turning the porous ionically conductive polymer film

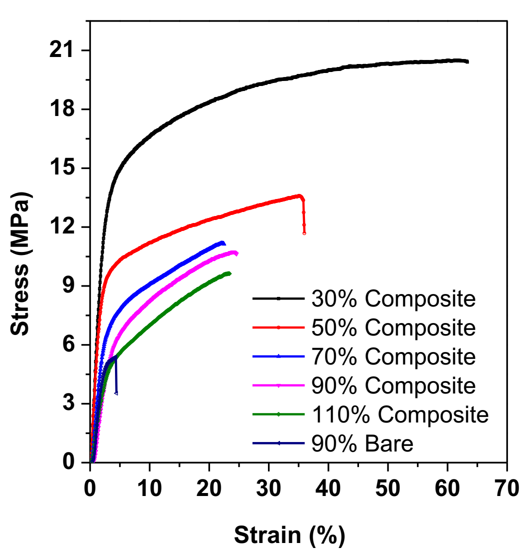

Fig. 5. Stress–strain curves of composite separator and bare PVDF–HFP membrane (90% PEG removal).

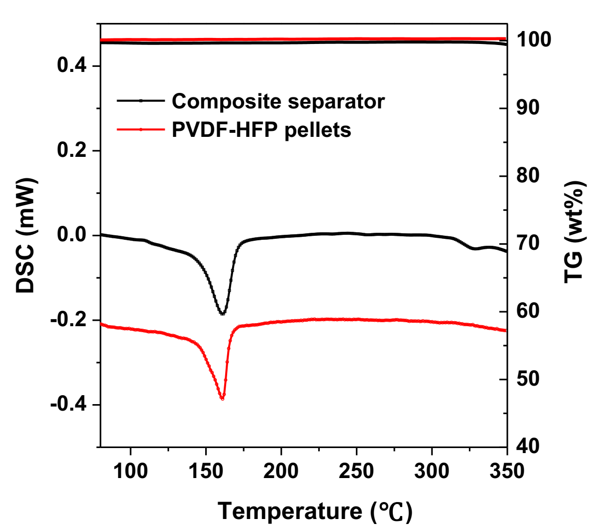

Fig. 6. DSC and TG curves of PVDF–HFP pallets, composite separator (90% PEG removal).

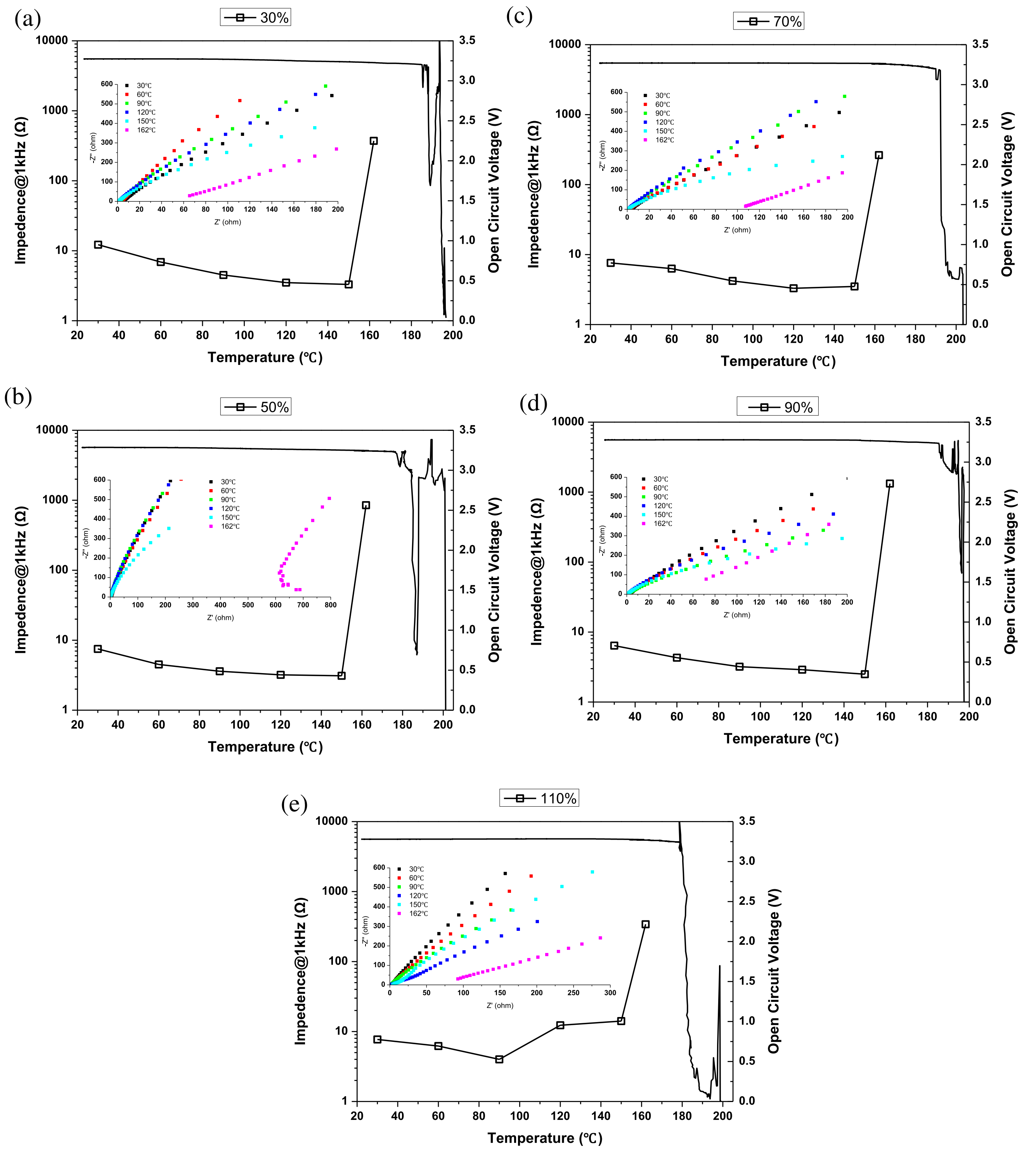

Fig. 7. Impedance at 1 kHz, the AC impedance spectra and open-circuit voltage (OCV) of the cell as a function of temperature: (a) 30%; (b) 50%; (c) 70%; (d) 90%; (e) 110%.

into a non-porous insulating layer between the electrodes [31]. The melted PVDF–HFP combined with ePTFE matrix tightly and formed a solid structure. All composite separators present similar morphology with the same heating process.

3.3. Thermo shrinkage performance

To prevent further electrochemical activity after shutdown and to maintain robust mechanical properties, the meltdown temperature of the separator should be higher than its shutdown temperature [34]. Fig. 9 presents the dimensional changes of different separators as a function of temperature investigated with TMA.

For composite separators, a slightly higher degree of thermal shrinkage occurred with higher content of PEG removal (Fig. 9), which may be related to the larger porosity. At the melting temperature of PVDF–HFP, the maximum length reduction is achieved and ranged from 4.7% (for 30% PEG removal) to 10.7% (for 110% PEG

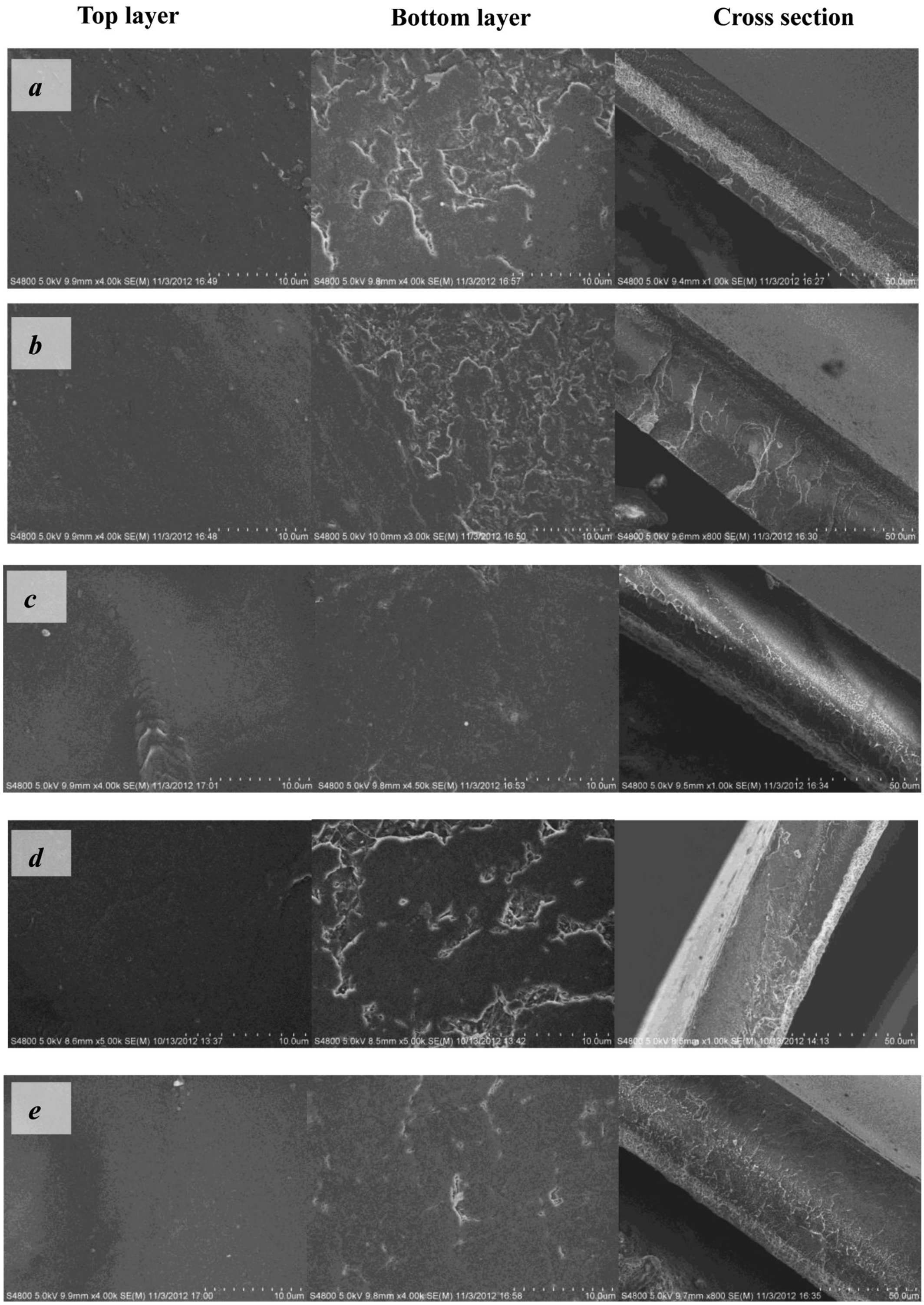

Fig. 8. FE-SEM photograph for composite separators after shutdown as a function of PEG removal: (a) 30%; (b) 50%; (c) 70%; (d) 90%; (e) 110%.

removal). Moreover, with the existing of ePTFE matrix, the composite separators preserved its integrity at the end of the TMA test (Fig. 9(a)) and could help to prevent the contact of the electrodes.

To further present the thermal shrinkage and the meltdown behavior of the composite separator, a digital camera was used to record the change of separators profile on a heating plate. Fig. 10 shows changes in the photograph as a function of temperature for composite separator. When temperature increases from 30 °C to 160 °C, composite separator undergoes tiny thermal shrinkage and ended with a dense and transparent structure caused by the melting of PVDF–HFP.

3.4. Electrochemical performance

The charge–discharge behaviors at different rates of the cells assembled with composite separator were investigated. Fig. 11

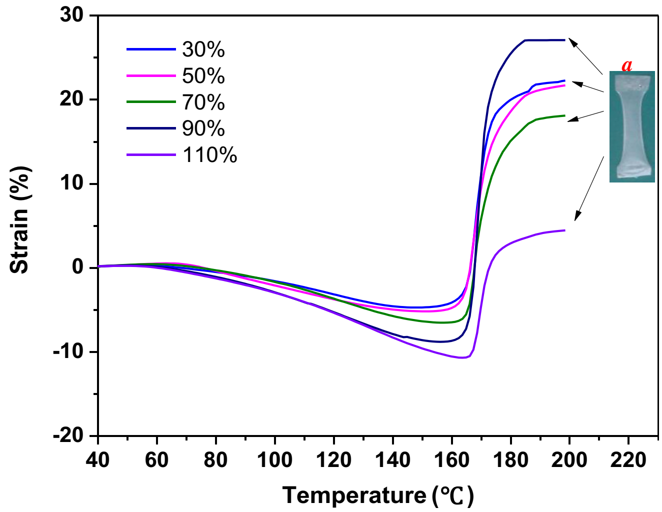

Fig. 9. Thermomechanical behavior of composite separators: (a) composite separator at the end of TMA test.

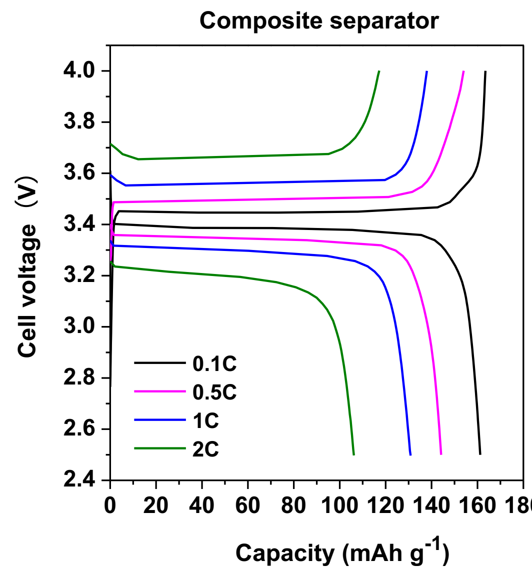

Fig. 11. Charge and discharge profiles of cells assembled the composite separator (90% PEG removal).

reveals that the discharge capacity of the cell is gradually decreased with higher discharge rate. The cell at the discharge rate of 0.1 C achieves the maximum discharge capacity of 161 mAh g^{-1}. At 2 C the cell keeps 66% of the discharge capacity at 0.1 C.

Fig. 12 shows the cyclability of the composite separator. After 50 cycles, the cell with the composite separator keeps 98.6% of its initial discharge capacity, making the separator a good candidate to be used in lithium-ion batteries.

The electrochemical stability window of the composite separator was evaluated by linear sweep voltammetry as shown in

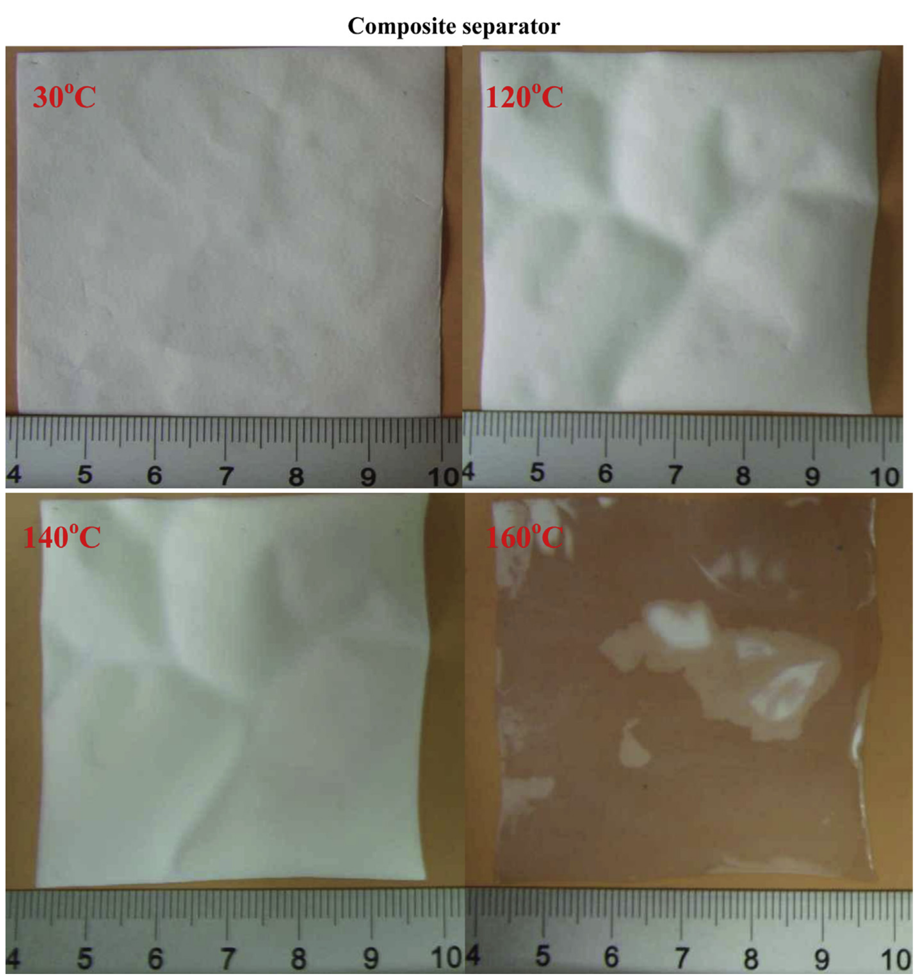

Fig. 10. Changes in the separator profile as a function of temperature, the initial dimension of separator is 6 cm × 6 cm at 30 °C.

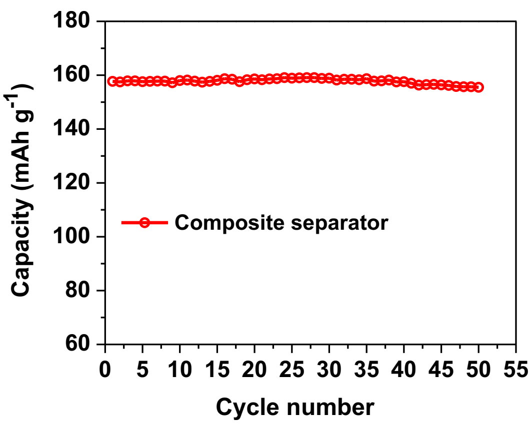

Fig. 12. Cycle performance of composite separator (90% PEG removal).

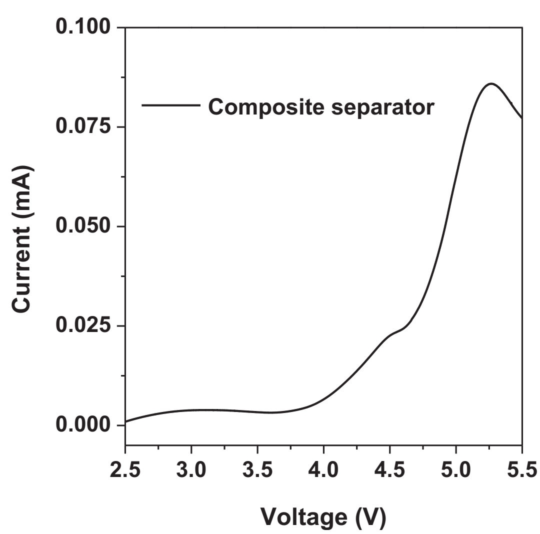

Fig. 13. Liner sweep voltammetry of the composite separator (90% PEG removal).

Fig. 13. It was observed that a very weak back-ground current was measured before 4 V, followed by a considerable increase in current flow which indicates the onset of electrochemical decomposition. Considering the electrode we use, it has sufficient electrochemical stability to endure the operating voltage of the battery system.

4. Conclusion

A new PVDF–HFP/ePTFE composite separator is reported in this work. It is found that the existing of ePTFE matrix can effectively improve the tensile strength and thermal stability of the separator. The porosity of composite separator could be controlled by varying the content of PEG removal. The composite separator has a function of shutdown at 162 °C and could maintain its integrity after the melting of PVDF–HFP while maintaining a low thermal shrinkage. Cells with this composite separator showed stable cycling performance and excellent rate capability.

Acknowledgment

This work is financially supported by the National Nature Science Foundation of China (51272200), Program for New Century Excellent Talents in University (NCET-12-0911) and National High Technology Research and Development Program (“863” Program) of China (2012AA053402).

References

[1] J.B. Goodenough, Y. Kim, Chemistry of Materials 22 (2009) 587–603.
[2] M. Baginska, B.J. Blaiszik, R.J. Merriman, N.R. Sottos, J.S. Moore, S.R. White, Advanced Energy Materials 2 (2012) 583–590.
[3] S.L. Li, L. Xia, H.Y. Zhang, X.P. Ai, H.X. Yang, Y.L. Cao, Journal of Power Sources 196 (2011) 7021–7024.
[4] D. Fu, B. Luan, S. Argue, M.N. Bureau, I.J. Davidson, Journal of Power Sources 206 (2012) 325–333.
[5] J.-R. Lee, J.-H. Won, J.H. Kim, K.J. Kim, S.-Y. Lee, Journal of Power Sources 216 (2012) 42–47.
[6] H.-S. Jeong, E.-S. Choi, S.-Y. Lee, J.H. Kim, Journal of Membrane Science 415 (2012) 513–519.
[7] J.-H. Cho, J.-H. Park, J.H. Kim, S.-Y. Lee, Journal of Materials Chemistry 21 (2011) 8192–8198.
[8] E.S. Choi, S.Y. Lee, Journal of Materials Chemistry 21 (2011) 14747–14754.
[9] K.J. Kim, J.-H. Kim, M.-S. Park, H.K. Kwon, H. Kim, Y.-J. Kim, Journal of Power Sources 198 (2012) 298–302.
[10] Y.S. Jung, A.S. Cavanagh, L. Gedvilas, N.E. Widjonarko, I.D. Scott, S.-H. Lee, G.-H. Kim, S.M. George, A.C. Dillon, Advanced Energy Materials 2 (2012) 1022–1027.
[11] J.-H. Park, W. Park, J.H. Kim, D. Ryoo, H.S. Kim, Y.U. Jeong, D.-W. Kim, S.-Y. Lee, Journal of Power Sources 196 (2011) 7035–7038.
[12] H. Li, X.-T. Ma, J.-L. Shi, Z.-K. Yao, B.-K. Zhu, L.-P. Zhu, Electrochimica Acta 56 (2011) 2641–2647.
[13] H.S. Jeong, S.Y. Lee, Journal of Power Sources 196 (2011) 6716–6722.
[14] Y.H. Liao, X.P. Li, C.H. Fu, R. Xu, L. Zhou, C.L. Tan, S.J. Hu, W.S. Li, Journal of Power Sources 196 (2011) 2115–2121.
[15] J.Y. Sohn, J.S. Im, J. Shin, Y.C. Nho, Journal of Solid State Electrochemistry 16 (2012) 551–556.
[16] J. Ding, Y. Kong, P. Li, J. Yang, Journal of the Electrochemical Society 159 (2012) A1474–A1480.
[17] S.-J. Chun, E.-S. Choi, E.-H. Lee, J.H. Kim, S.-Y. Lee, S.-Y. Lee, Journal of Materials Chemistry 22 (2012) 16618–16626.
[18] H. Xiang, J. Chen, Z. Li, H. Wang, Journal of Power Sources 196 (2011) 8651–8655.
[19] M.-H. Ryou, Y.M. Lee, J.-K. Park, J.W. Choi, Advanced Materials 23 (2011) 3066–3070.
[20] L.C. Zhang, X. Sun, Z. Hu, C.C. Yuan, C.H. Chen, Journal of Power Sources 204 (2012) 149–154.
[21] C.G. Wu, M.I. Lu, H.J. Chuang, Polymer 46 (2005) 5929–5938.
[22] T.-H. Young, L.-P. Cheng, D.-J. Lin, L. Fane, W.-Y. Chuang, Polymer 40 (1999) 5315–5323.
[23] L.-P. Cheng, T.-H. Young, L. Fang, J.-J. Gau, Polymer 40 (1999) 2395–2403.
[24] J. Hwang, S.K. Jeong, K.S. Nahm, A.M. Stephan, European Polymer Journal 43 (2007) 65–71.
[25] J.-J. Kim, J.R. Hwang, U.Y. Kim, S.S. Kim, Journal of Membrane Science 108 (1995) 25–36.
[26] Q. Shi, M. Yu, X. Zhou, Y. Yan, C. Wan, Journal of Power Sources 103 (2002) 286–292.
[27] V. Gentili, S. Panero, P. Reale, B. Scrosati, Journal of Power Sources 170 (2007) 185–190.
[28] P. Arora, Z.M. Zhang, Chemical Reviews 104 (2004) 4419–4462.
[29] X. Huang, Journal of Power Sources 216 (2012) 216–221.
[30] C.L. Cheng, C.C. Wan, Y.Y. Wang, M.S. Wu, Journal of Power Sources 144 (2005) 238–243.
[31] G. Venugopal, J. Moore, J. Howard, S. Pendalwar, Journal of Power Sources 77 (1999) 34–41.
[32] G. Venugopal, Journal of Power Sources 101 (2001) 231–237.
[33] I. Uchida, H. Ishikawa, M. Mohamedi, M. Umeda, Journal of Power Sources 119 (2003) 821–825.
[34] K.W. Song, C.K. Kim, Journal of Membrane Science 352 (2010) 239–246.